Aero-Optical Analysis of Compressible Flow Over an Open Cavity

Philip E. Cassady,* Stanley F. Birch,† and P. John Terry‡
Boeing Aerospace, Seattle, Washington

The optical rays that form the image of an object viewed through an open port in a high-altitude transonic aircraft are refracted by the unsteady density variations in a compressible turbulent shear layer. A time-dependent, two-dimensional Navier-Stokes computer code has been used to model the flowfield including the reattachment process. Optical ray tracing and image formation codes using fast Fourier transforms have been developed to generate both intensity profiles and intensity contours at the focal plane. Values of centerline intensity loss, steady and unsteady beam steering, and image distortion were extracted from the results of calculations made over a range of Mach numbers between 0.6 and 0.8 at altitudes of 40,000–50,000 ft. Two-dimensional predictions of image steering agree with those generated by a less detailed self-similar model. Image distortion was found to be almost entirely made up of wavefront tilt without appreciable higher-order distortion. Higher-order image distortion is shown to depend on the details of coherent structures in the shear layer that are presently very difficult to predict theoretically.

Introduction

AT the present time, there are both civilian[1] and military[2] programs using an optical sensor mounted aboard a high-altitude aircraft platform where the presence of warm material windows introduce unacceptable background noise in the infrared wavelength regions of interest and geometric constraints limit the use of cooled windows. The optical rays that form an image of an object viewed through an open port in the side of a high-altitude transonic aircraft will traverse the compressible turbulent shear layer that forms between the ambient external flowfield and the air internal to the optical cavity on the airplane. These optical rays are refracted by the unsteady density variations in the turbulent flow and diffracted by the fine-scale structure of the turbulence.[3,4]

Analyses of the degradation of optical beams passing through turbulent media involve two coupled models: a fluid dynamic description of the turbulent medium and an analysis of optical propagation through the described distribution of gaseous properties. This paper uses recent advances in computer capabilities that allow a more realistic description of compressible turbulent mixing layers. Then, optical ray tracing and propagation analyses using fast Fourier transforms are used to calculate intensity profiles and intensity contours of optical images in a focal plane located behind a turbulent mixing layer.

The scattering of electromagnetic waves by the turbulent atmosphere has been a subject of interest to astronomers and applied mathematicians for many years.[5] Investigations of optical transmission through turbulent boundary layers using analogous methods showed a significant loss in optical resolving power.[6,7] Similar analyses have been used to determine the medium quality requirements for flowing gas lasers.[3] The discipline of aero-optics has evolved combining the fields of fluid dynamics and electromagnetic wave propagation.[4,8]

Presented as Paper 87-1399 at the AIAA 19th Fluid Dynamics, Plasma Dynamics, and Lasers Conference, Honolulu, HI, June 8–10, 1987; received July 30, 1987; revision received June 1, 1988.

*Senior Principal Engineer. Associate Fellow AIAA.
†Principal Engineer. Member AIAA.
‡Specialist Engineer.

Table 1 Classification of aero-optical effects

Optical degradation	Flow disturbance scale size	Optical effect
Large angle scattering	<< Optical aperture	Reduce image brightness Strehl ratio
Defocus	< Optical aperture	Temporal and spatial image spread
Jitter (unsteady steering)	= > Optical aperture	Unsteady image wander
Steady steering (tilt)	= > Optical aperture	Steady image displacement

The application of modern fluid dynamic analyses of turbulent mixing layers to aero-optical phenomena introduces a new emphasis on the fluid dynamic predictions. Classically, the aeronautical engineer has been interested in accurate prediction of pressures and velocities in regions of the flowfield near boundaries because these flowfield properties determine the forces and moments on airfoils. Aero-optical analysis places a new importance on the accurate prediction of steady and unsteady density fields in regions of the flow traversed by optical rays that may be far from aerodynamic surfaces. A similar interest also is represented in recent studies of turbulent combustion phenomena.

Optical degradations introduced by turbulent flowfields may be classified by the ratio of the size of the flow-induced density disturbance to the size of the optical aperture as shown in Table 1. Flow disturbances much smaller than the aperture size scatter optical energy by large angles, causing some to miss the optical aperture and thereby producing an attenuation of image intensity that is measured by a decrease in the Strehl ratio.[3] Larger flow disturbances that are a fraction of the size of the optical aperture redirect optical rays within the aperture, introducing steady and unsteady higher-order image distortion that affects the size and shape of the intensity distribution in the image plane. Flow disturbances that are equal or larger in size than the aperture steer the rays in a relatively uniform manner across the aperture, introducing steady and unsteady steering or wavefront tilt that causes movement of the image in the focal plane.

The objective of the research reported in this paper is to analyze the optical distortions that are caused by a compress-

ible, unsteady turbulent shear layer across an open cavity. The approach is described in the following two sections. Results that meet the stated objective are described and discussed in the fourth section and several conclusions and recommendations are presented in the final section.

Flowfield Analyses

Three theoretical models of the turbulent compressible shear layer over an open cavity were used in this study. The first model addressed only the shear layer between the external stream and the quiescent cavity air without consideration of the cavity internal flowfield, separation process, or reattachment process. This self-similar analytical model of shear layer growth[9] was initially used to examine the magnitude of optical effects and to provide a physical understanding of the phenomena. This model used an empirically derived shear layer velocity profile[10] and a measured compressible shear layer growth rate,[11] as

$$U = \frac{u}{u_1} = \frac{1-\cos\pi\theta/\theta_1}{2} \tag{1}$$

where u is the flow velocity, θ the angular position in the shear layer referred to the origin of the shear layer and its cavity side edge, subscript 1 the freestream conditions, and θ_1 the empirically derived shear layer growth angle. The steady density field was calculated from this velocity field using the Crocco relation,

$$\frac{\rho}{\rho_1} = \frac{h_1/H_1}{h_2/H_1 + (1-h_2/H_1)U - (1-h_1/H_1)U^2} \tag{2}$$

where ρ is the density, h the static enthalpy, and H the total enthalpy. Variation of the refractive index is related to density variation through the Gladstone-Dale relation. A mixing length turbulence model was included. The overall angular light ray deviation was calculated by numerically integrating the nonlinear equation describing a light ray path through the disturbed medium,

$$\frac{d\alpha}{d\theta} = \frac{\pi\beta\rho_1 A(C+2DU)\sin(\pi\theta/\theta_1)\tan(\alpha-\theta)}{2\theta_1\rho_s(B+CU+DU^2+A\beta\rho_1/\rho_s)(B+CU+DU^2)} \tag{3}$$

where α is the angular deviation of the ray, β the Gladstone-Dale constant referred to ρ_s, and

$$A = h_1/H_1 = [1 + (\gamma-1)M_1^2/2]^{-1} \tag{4}$$

$$B = h_2/H_1 \tag{5}$$

$$C = 1 - B \tag{6}$$

$$D = A - 1 \tag{7}$$

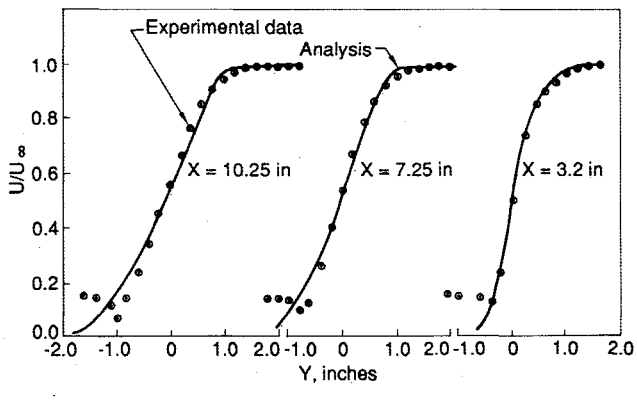

Fig. 1 Comparison of shear layer velocity measurements with parabolized Navier-Stokes predictions (Mach 0.8).

Air on the cavity side of the mixing layer was assumed to be isentropically stagnated from freestream conditions. Since this self-similar shear layer model has no length scale, it cannot include the effect of an incoming boundary layer, the separation process, the cavity internal flowfield, or the reattachment process.

The second theoretical flow model used a two-dimensional compressible boundary-layer analysis to include the effects of an upstream boundary layer, the separation process, and the shear layer curvature.[12] The computer code used a parabolized form of the Navier-Stokes equations limited to modeling flows with a predominant flow direction and with no recirculation in that direction. An advanced turbulence model that solves partial differential equations for turbulence kinetic energy and turbulence energy dissipation rate[13] was used, and the discretized nonlinear equations were solved using an iterative fully implicit marching scheme,

$$\frac{\partial(\rho u)}{\partial x} + \frac{\partial(\rho v)}{\partial y} = 0 \tag{8}$$

$$\frac{\partial(\rho u^2)}{\partial x} + \frac{\partial(\rho uv)}{\partial y} = \frac{\partial}{\partial y}\left[(\mu_t + \mu)\frac{\partial u}{\partial y}\right] \tag{9}$$

$$\frac{\partial(\rho uH)}{\partial x} + \frac{\partial(\rho vH)}{\partial y} = \frac{\partial}{\partial y}\left[\left(\frac{\mu_t}{\sigma_h} + \frac{\mu}{Pr}\right)\frac{\partial H}{\partial y}\right] \tag{10}$$

$$\frac{\partial(\rho uk)}{\partial x} + \frac{\partial(\rho vk)}{\partial y} = \frac{\partial}{\partial y}\left[\left(\frac{\mu_t}{\sigma_k} + \mu\right)\frac{\partial k}{\partial y}\right] + \mu_t\left(\frac{\partial u}{\partial y}\right)^2 - \rho\epsilon \tag{11}$$

$$\frac{\partial(\rho u\epsilon)}{\partial x} + \frac{\partial(\rho v\epsilon)}{\partial y} = \frac{\partial}{\partial y}\left[\left(\frac{\mu_t}{\sigma_\epsilon} + \mu\right)\frac{\partial \epsilon}{\partial y}\right] + C_1\frac{\epsilon}{k}\left(\frac{\partial u}{\partial y}\right)^2 - C_2\frac{\epsilon^2}{k} \tag{12}$$

$$\mu_t = C_D\rho\frac{k^2}{\epsilon} \tag{13}$$

where u and v are the two-dimensional velocity components, μ the laminar viscosity, μ_t the turbulent viscosity, H the total enthalpy, Pr the laminar Prandtl number, σ_h the turbulent Prandtl number, k the turbulence kinetic energy, and ϵ the turbulence energy dissipation rate. Five constants were chosen: $C_D = 0.09$, $C_1 = 1.44$, $C_2 = 1.92$, $\sigma_k = 1$, and $\sigma_\epsilon = 1.30$.

This code was used to model the aerodynamic flowfield associated with the shear layer across a 33 cm long wall cavity in a transonic wind tunnel operating at Mach numbers between 0.5 and 0.8. The calculations accurately predicted measured profiles of pressure and velocity. A comparison between measured and predirected velocity profiles in this shear layer is shown in Fig. 1. Although density predictions were not directly verified, these results indicate the ability of this code to predict steady flowfield properties. Steady flow density profiles for the optical ray tracing computations were calculated from the compressible flow equations. This two-dimensional parabolized Navier-Stokes model did not include unsteady effects, the cavity internal flowfield, or the effects of the flow reattachment process at the downstream end of the cavity.

The third theoretical flow model, an unsteady, compressible, two-dimensional Navier Stokes analysis, using the split explicit predictor-corrector algorithm of MacCormack and an algebraic eddy viscosity turbulence model, included the internal cavity flowfield, the reattachment process, and unsteady flow effects.[14] The equations were written in a strong conservation form for a nonorthogonal, body-fitted, transformed coordinate system. A finite-volume formulation was used in the derivation of the finite-difference equations. The effects of turbulence were simulated with a Baldwin-Lomax turbulence model and wall functions were used to minimize the mesh requirements in the steep gradients near solid surfaces. The ability of this code to predict density variations was not experimentally verified. However, its demonstrated ability to pre-

dict flow stability and reattachment location[14] offered the best capability to predict complex shear layer flow properties that was readily available. Density profiles calculated for Mach 0.75 flow of air at 40,000 ft altitude are shown in Fig. 2. The large-density disturbance associated with the reattachment process is apparent.

Flowfield property variations calculated from these analyses were used with optical analyses to provide estimates of large-angle scattering and unsteady optical steering. Since the turbulence models used in these analyses were not capable of predicting the evolution of coherent structures in the shear layer that are a fraction of the size of the optical aperture, optical analyses based on them do not predict higher-order image distortions.

Optical Analyses

An optical ray trace code was used to follow individual rays in a bundle from a flat phase front located far away from the influence of the shear layer, through the shear layer, and onto an optical aperture located on the cavity side of the shear layer. The flat phase front initial condition with uniform intensity distribution and uniform phase distribution represents a wave from a distant point source. Such near-field calculations using geometrical optics are suitable for the ranges of wavelengths, turbulence scale sizes, and optical pathlengths through shear layer flowfields of interest.[15] After the rays entered the optical aperture, a full two-dimensional Fraunhofer diffraction calculation was used to develop the image of the distant point source through ideal focusing optics.

The ray propagation equation was integrated for each optical ray as it progressed through the refractive index variations associated with the time-dependent density field prescribed by the flowfield calculations described above. The optical pathlength was calculated for each ray in a bundle that uniformly covered the optical aperture, and a wavefront distortion was calculated at the aperture plane, which was located at a prescribed position and angle inside the wall cavity. Using these rays, the near-field optical pathlength difference (OPD) was calculated as a function of time and position in this aperture plane, and the wavefront tilt, defocus, and rms OPD variation were determined. The Strehl ratio, which is a measure of image centerline intensity loss,[3] was calculated from the tilt-corrected rms OPD variation σ using the Merechal approximation,

$$I/I_0 = \exp - k^2\sigma^2 \qquad (14)$$

where k is the optical wave number. Since the calculated centerline intensity loss was very small, the Strehl ratio calculation was not corrected for defocus or intensity aberrations. The image steering angle caused by wavefront tilt was calculated from the least squares fit to the OPD distribution, which gives the wavefront tilt, and also from the translation of the peak intensity in the image plane that was caused by this wavefront tilt.

The aberrated wavefront was projected into the image plane using a propagation code based on a discrete two-dimensional fast Fourier transform algorithm. A computer plotting routine was used to present both intensity profiles and intensity contours of the image in the focal plane at times for which flowfield data were calculated.

Results and Discussion

Calculations were made for air over a range of Mach numbers between 0.6 and 0.8 and standard altitudes of 40,000–50,000 ft. Various look angles between the flow axis and optical axis were examined. The image of a distant point source (plane illuminating phase front) on the focal plane of an ideal optical system located within the cavity was calculated.

Since the self-similar model of the flowfield has no length scale, its density profile can introduce only optical steering.

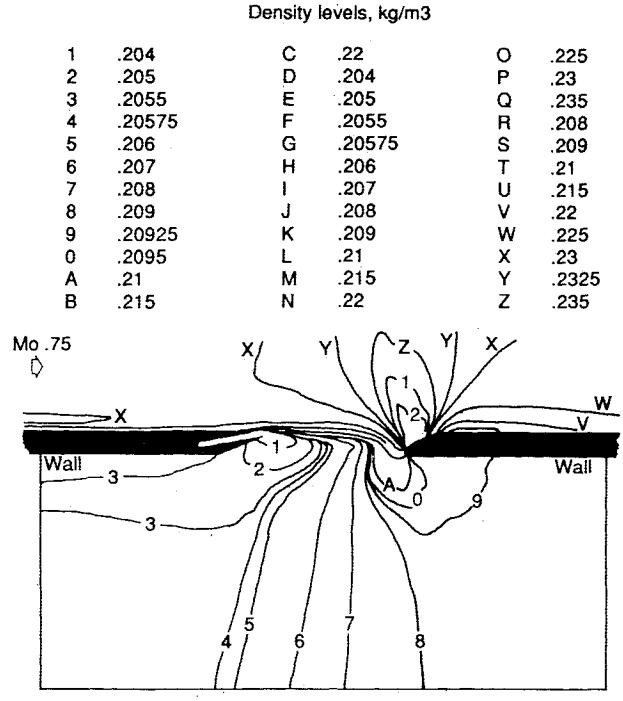

Fig. 2 Density contours for compressible flow over open cavity (40,000 ft, Mach 0.75).

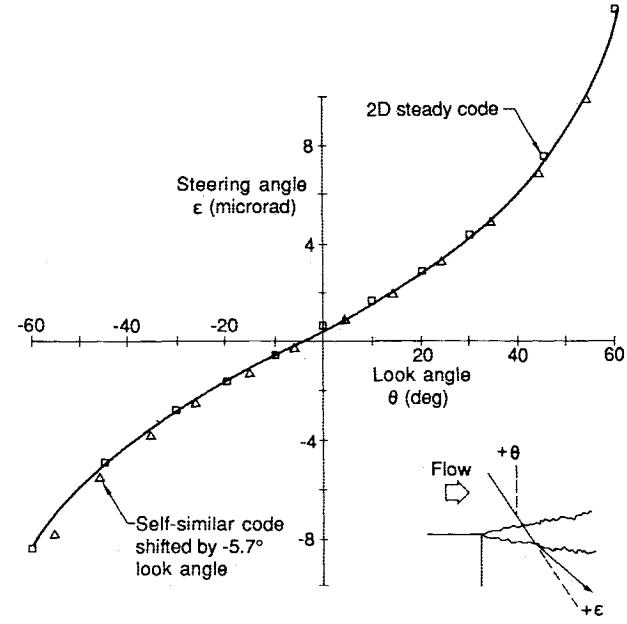

Fig. 3 Steady image steering through compressible turbulent shear layer (45,000 ft, Mach 0.8).

Unsteady beam steering was modeled parametrically by including motion of the shear layer reattachment point with magnitudes derived from shear layer measurements taken with a schlieren system in a small transonic wind tunnel. Estimates of higher-order image distortions were generated by forcing the simple shear layer profile to follow shape variations that were taken from similar schlieren photographs.

Calculations of optical beam steering using the self-similar flowfield model and the steady two-dimensional flow model are shown in Fig. 3. The two-dimensional model calculation included the effect of a 2.5 cm thick upstream turbulent boundary layer. Predictions of steering angle variation with look angle using the self-similar model agree with those from the more complex two-dimensional model when a small shift in shear layer location is included. It is remarkable that the

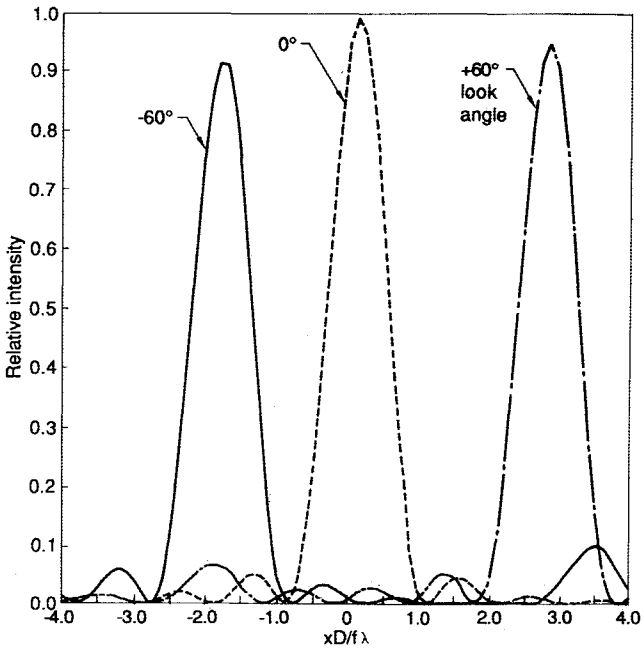

Fig. 4 Focal plane intensity profiles of a distant point source viewed through a compressible turbulent shear layer at various look angles (square aperture, 3 μm wavelength, 45,000 ft, Mach 0.8).

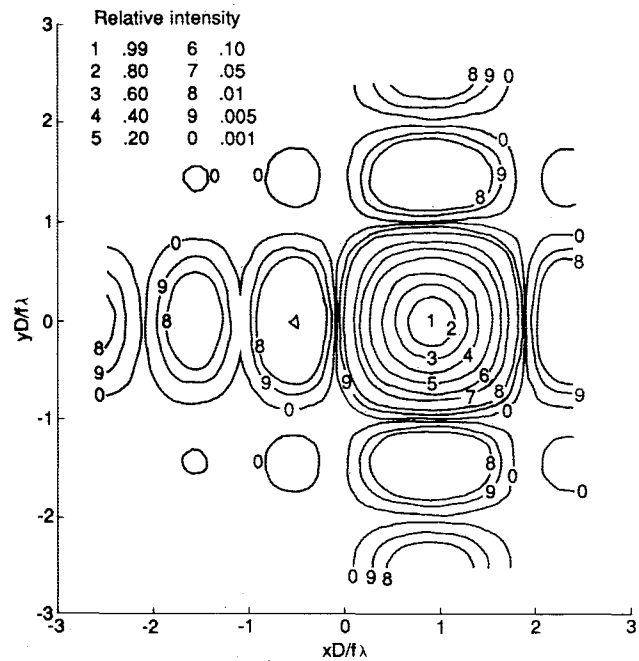

Fig. 5 Focal plane intensity contours of distant point source viewed through compressible turbulent shear layer (square aperture, 3 μm wavelength, +30 deg look angle, 45,000 ft, Mach 0.8).

self-similar model is capable of predicting this nonlinear variation with only a small angular shift to account for the effects of the upstream boundary layer developing into a shear layer[12] and flowfield curvature. Although the two-dimensional flow model allows flowfield curvature and attendant optical distortion, the near-field OPD was found to be almost entirely made up of wavefront tilt without appreciable higher-order distortion.

The Strehl ratio at 3.0 μm wavelength, calculated from the tilt-corrected rms OPD using Eq. (14) for the conditions shown in Fig. 2, was 0.98, indicating very little large-angle scattering. Because of its exponential dependence on the square of the wavelength shown in Eq. (14), the Strehl ratio would be considerably decreased at shorter wavelengths in the visible spectrum. This effect is shown clearly in Fig. 11 on p. 36 of Ref. 4. Although this figure was calculated for a turbulent boundary layer rather than the free turbulent shear layer considered here, it also indicates only a few percent on axis intensity loss at 3 μm wavelength for Mach number and altitude conditions shown in Fig. 2.

Focal plane intensity profiles with propagation directions normal to the freestream and inclined 60 deg in the upstream and downstream directions are shown for 45,000 ft altitude conditions in Fig. 4. The dimensionless abscissa is the deviation angle times the aperture width divided by the wavelength. The peak image intensity is lowered for the inclined look angles by the increased OPD variations over the longer tilted pathlengths, but the image does not appear distorted. The image spot size is essentially determined by the diffraction pattern of the optical aperture with its location shifted corresponding to the tilt introduced into the near-field OPD by the shear layer.

A focal plane intensity contour map is shown in Fig. 5 for the same flow conditions and a look angle of 30 deg upstream. Similar dimensionless coordinates are used in this figure. The calculation was done for a square aperture to be consistent with the two-dimensional flow analysis. For these conditions, within the limitations of the model, the flow does not appreciably distort the image and the image intensity contour is essentially determined by the diffraction pattern of the square aperture displaced by tilt introduced into the near-field OPD by the shear layer. Comparison of the y-axis variation, which was completely free of flowfield induced distortion in the two-dimensional flowfield model, to the x-axis variation, which included the full flowfield distortion effect, reveals a very small redistribution of image intensity into the higher pattern orders. This redistribution will be accentuated when the optical wavelength is shortened because the OPD, measured in units of optical wavelengths, will correspondingly increase for a given flow disturbance.

Unsteady flow results calculated using the two-dimensional model show unsteady beam steering that has a temporal period similar to the time required for a flow disturbance to convect across the open cavity and then acoustically feed back upstream to the flow detachment point. The magnitude of the unsteady steering component was found to be much smaller than the steady component of beam steering for this configuration.

The optical calculations were found to be very sensitive to the accuracy of the fluid dynamic density calculations in the freestream regions of the flow because optical traverses through these regions involve long path lengths, and small local differences in optical pathlength can accumulate to appreciable OPD values. The flowfield as shown in Fig. 2 was partitioned into three regions to investigate this problem. Separate calculations revealed negligible optical effects caused by the very low Mach number internal cavity region. The shear layer region introduced appreciable optical effects, as expected. In addition it was found that a streamwise density variation as small as 0.43% across the aperture dimension at a freestream location 10 m away from the external surface introduced 2.5 μrad of beam steering. This level of freestream definition accuracy, which was sufficient to provide stable, convergent fluid dynamic solutions for conventional aerodynamic calculations, was found to be insufficient to support aero-optical calculations. One must be very careful either to calculate density levels in the freestream very accurately or to truncate the optical integrations in a manner that avoids unrealistic density variations. Optical calculations reported in this paper were truncated to avoid the unrealistic streamwise density gradient.

The two-dimensional analyses described here have not been

used to model the internal flowfield of a cavity with optical equipment installed. The shape of such equipment and the flow around it require the use of a three-dimensional model for adequate description.

The present analysis is unable to accurately predict higher-order image distortion because the flow analyses are unable to realistically model shear layer structures of the size that will introduce higher-order image distortions. It will be necessary to accurately calculate the generation and evolution of large coherent structures in the shear layer to accurately predict the effects of higher-order image distortions.

A specific flow configuration has been chosen in this paper to illustrate the application of the present aero-optical analysis. As described in Ref. 14, the flow separation and reattachment geometry depicted in Fig. 2 was carefully designed to reduce flow disturbances and unsteadiness that could adversely affect the optical quality of a beam entering the cavity. This design is new and is being patented. An optical turret is an earlier design approach intended to provide a large field of view from a high-altitude transonic aircraft. Even with extensive fairing this design introduces inviscid flowfield lensing and wakes[4] that have not been included in the analyses reported here. Another approach uses a perforated fence to deflect and artificially thicken the upstream boundary layer, provide a thick turbulent shear flow that is relatively insensitive to the separation and reattachment processes, and suppress the formation of cavity acoustic resonances. This approach has been used on the Kuiper Airborne Observatory.[1] The geometry depicted in Fig. 2 was designed to avoid the thick turbulent shear flow generated by such an upstream fence. Although the Kuiper aircraft flies at a similar altitude and Mach number, its flow configuration is considerably different than that of the design reported in this paper. Because of our interest in maintaining a narrow shear flow, we have not pursued the fence design approach and have not performed aero-optical analyses of the Kuiper flow configuration.

Conclusions and Recommendations

The aero-optical effects of the turbulent compressible shear layer across an open viewport in a high-altitude transonic aircraft have been calculated within the limitations of the two-dimensional, turbulent, compressible Navier-Stokes fluid dynamic analyses used. The primary aero-optical effect was found to be beam steering. A simple self-similar model predicted the nonlinear variation of this beam steering as well as more complex two-dimensional flow models. Very little higher-order image distortion was predicted since the flow analyses were unable to realistically model diffractive scattering structures in the shear layer. It is recommended that large eddy simulation codes be extended to applicable flow regimes to allow the more accurate prediction of higher-order aero-optical effects. Experimental verifications of unsteady density distributions are also required, particularly for the transonic, three-dimensional flowfields of interest here.

Acknowledgment

This work was funded by Boeing Aerospace and Boeing Commercial Airplanes.

References

[1]Cameron, R. M., Bader, M., and Moble, R. E., "Design and Operation of the NASA 91.5 cm. Airborne Telescope," *Applied Optics,* Vol. 10, Sept. 1971, pp. 2011–2015.

[2]Merrifield, J. T., "Boeing Receives Flight Hardware for Airborne Optical Adjunct Tests," *Aviation Week and Space Technology,* Vol. 125, No. 14, Nov. 1986, pp. 84–86.

[3]Sutton, G. W., "Effect of Turbulent Fluctuations in an Optically Active Fluid Medium," *AIAA Journal,* Vol. 7, Sept. 1969, pp. 1737–1743.

[4]Gilbert, K. G. and Otten, L. J. (eds.), *AIAA Progress in Astronautics and Aeronautics: Aero-Optical Phenomena,* Vol. 80, AIAA, New York, 1982.

[5]Tatarski, V. I., *Wave Propogation in a Turbulent Medium,* Dover, New York, 1967.

[6]Stine, H. A. and Winovich, W., "Light Diffusion Through High Speed Turbulent Boundary Layers," NACA RM A56B21, Feb. 1956.

[7]Wolters, D. J., "Aerodynamic Effects on Airborne Optical Systems," McDonnell Aircraft Co., St. Louis, MO, Rept. MDC A2582, 1973.

[8]Sutton, G. W., "Aero-Optical Foundations and Applications," *AIAA Journal,* Vol. 23, Oct. 1985, pp. 1525–1537.

[9]Schlichting, H., *Boundary Layer Theory,* McGraw-Hill, New York, 1979, pp. 737–738.

[10]Peters, C. E. and Phares, W. J., "An Integral Turbulent Kinetic Energy Analysis of Free Shear Flows," *Free Turbulent Shear Flows,* NASA SP-321, 1972, pp. 577–628.

[11]Maydew, R. C. and Reed, J. F., "Turbulent Mixing of Compressible Free Jets," *AIAA Journal,* Vol. 1, June 1963, pp. 1443–1444.

[12]Birch, S. F., "The Effect of Initial Conditions on High Reynolds Number Jets," AIAA Paper 83-1681, July 1983.

[13]Launder, B. E. and Spaulding, D. B., "The Numerical Computation of Turbulent Flows," *Computer Methods in Applied Mechanics and Engineering,* Vol. 3, No. 2, March 1974, pp. 269–289.

[14]Om, D., "Navier-Stokes Simulation of Flow Past an Open Cavity," AIAA Paper 86-2628, Oct. 1986.

[15]Hornstein J. and Fainberg, J., "Ray Methods in Random Media," *Atmospheric Transmission,* Vol. 277, 1981, pp. 16–25.